Eur. Phys. J. D **13**, 221–229 (2001)

THE EUROPEAN PHYSICAL JOURNAL D

EDP Sciences
© Società Italiana di Fisica
Springer-Verlag 2001

Implementation of a sapphire cell with external electrodes for laser excitation of a forbidden atomic transition in a pulsed E-field

E. Jahier, J. Guéna, Ph. Jacquier, M. Lintz, and M.A. Bouchiat[a]

Laboratoire Kastler Brossel[b], Département de Physique de l'École Normale Supérieure, 24 rue Lhomond, 75231 Paris Cedex 05, France.

Received 15 September 2000

Abstract. We demonstrate the production of an electric field *inside* a high temperature cesium vapor cell with *external* electrodes. This external control of the electric field, which is not possible with a glass cell in presence of a cesium vapor, is achieved using a cell made of sapphire, and is of particular interest for our ongoing Parity Violation experiment. We describe the main components and the implementation on the set-up, including the pulsed high voltage generator. With pulse duration not exceeding 200 ns the system provides a reversible longitudinal **E**-field of up to 2 kV/cm in the vapor at a density of $\sim 2 \times 10^{14}$ at/cm^3 without discharge. Atomic signals attest the application of the electric field in the cell, with the predicted value. Further improvements obtained with sapphire cells are also presented.

PACS. 32.80.Ys Weak-interaction effects in atoms – 33.55.Be Zeeman and Stark effects – 41.20.Cv Electrostatics; Poisson and Laplace equations, boundary-value problems

1 Introduction

The spectroscopy of emission lines and optical anisotropies of atomic vapors submitted to electric or magnetic fields has played a major role in understanding atomic physics (Zeeman, Paschen-Back, Faraday and Stark effects). Some fine magneto-optical effects such as the non-linear Faraday effect are still under investigation [1,2].

At present, the application of static *magnetic* fields **B** in an atomic vapor has become an essential tool for today's atomic physics and quantum optics, the most popular illustrations being the magnetic and the magneto-optical traps used for obtaining Bose-Einstein condensation [3,4].

In high precision experiments devoted to the study of discrete symmetries at low energy, the application of an *electric* field **E** on atomic samples has been a major tool for more than 20 years. There are mainly two kinds of such experiments: (i) measurement of Parity Violation (PV) originating from weak neutral currents (Z^o exchange), by the Stark interference method in forbidden M_1 atomic transition [5], and (ii) test of Time Reversal Violation *via* the search for a permanent E.D.M. (electrical dipole moment) in stable systems [6], predicted by theories beyond the Standard Model.

Our PV experiment in progress at ENS is of the first kind, and is conducted using a cesium vapor cell. The experimental configuration consists of two collinear laser beams (the pump and the probe) and a 2 kV/cm **E**-field in the same direction along an interaction length of 8 cm, at a vapor pressure of a few mtorr. For a pump laser frequency resonant with the highly forbidden 6S–7S transition in cesium, the excitation rate of the ground state atoms is controlled by the **E**-field and is proportional to E^2. The two light beams and the **E**-field are pulsed. The pulse duration of the latter has to be long compared to the pump pulse duration. As a matter of fact, the application of an electric field in a cell becomes non trivial when the cell contains a chemically aggressive alkaline vapor, *e.g.* cesium. In particular inside a *glass* cell, internal electrodes are needed if one wants to apply an **E**-field either static, or quasi-static at the time scale defined by the pump beam pulse. In this paper, we describe the possibility offered by sapphire cells to control the electric field in the vapor with *external* electrodes, and to overcome other difficulties raised by glass cells in the conditions of our PV experiment in cesium.

In Section 2, we summarize our reasons for choosing a new kind of cell. Then (Sect. 3), we outline the main difference between glass and sapphire cells, with regard to the electrical conductivity, and its consequences for generating the **E**-field. Next (Sect. 4), we describe the practical realization, which is divided into three parts: (i) the oven containing the cesium cell, (ii) the electrode configuration, and (iii) the production of reversible high voltage pulses that feed the electrodes. Section 5 is devoted to the

[a] e-mail: marianne@lkb.ens.fr

[b] Laboratoire de l'École Normale Supérieure et de l'université Pierre et Marie Curie, associé au CNRS (UMR 8552).

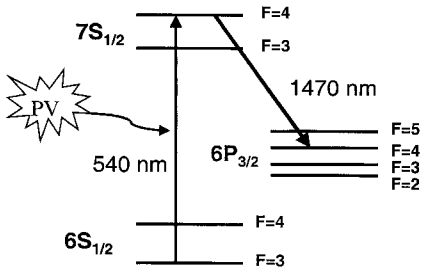

Fig. 1. Energy levels of the Cs atom. The pump laser is tuned to the forbidden $6S_F \rightarrow 7S_{F'}$ transition, and the probe is tuned to the allowed $7S_{F'} \rightarrow 6P_{3/2F''}$. Parity violation occurs during the 6S–7S excitation, and the information left in the 7S excited state is read by the probe pulse.

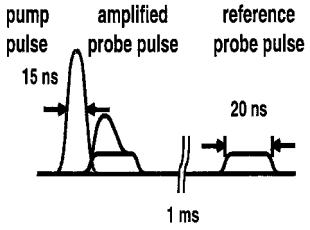

Fig. 2. Time sequence of the experiment. The probe pulse consecutive to the excitation pulse is amplified by stimulated emission. The second probe pulse sent 1 ms later, serves as a reference without excited atoms.

experimental results: diagnostic of the electric field in the cell, and further improvements over previous glass cells obtained by our exploiting thermal and mechanical properties of sapphire. The difficulty remaining with a photoinduced electron emission is mentioned. Lastly (Sect. 6) we bring out the new perspective opened by extending this work to the transverse field configuration.

2 Motivation for sapphire cells

Our current Parity Violation experiment in cesium is of the pump-probe kind. The Cs levels involved are represented in Figure 1, while Figure 2 shows the timing of the experiment. In presence of a longitudinal electric field **E**, the 6S−7S highly forbidden transition ($\lambda = 539$ nm) is excited in a vapor, with a linearly polarized pump pulse (repetition rate 120 Hz). A few ns later, a second, collinear pulse, with the same initial polarization, but tuned to the allowed 7S−$6P_{3/2}$ ($\lambda = 1.47$ μm), probes the anisotropy (electronic orientation or alignment) created in the 7S state ($\tau_{7S} = 48$ ns) by the pump pulse. We detect this anisotropy by analyzing the probe polarization after propagation and amplification by stimulated emission in the excited vapor. This is done very precisely by comparison with a reference pulse sent 1 ms later, when all excited atoms have decayed (see [7] for details about the experiment).

The highly forbidden 6S–7S transition is chosen [5] in order to greatly enhance the asymmetry resulting from the PV electroweak interference during the excitation, and the transition rate is controlled by the longitudinal electric field causing Stark mixing of S and P states. The reversal of the electric field provides a very powerful signature for the PV signal, whose sign reverses when **E** is reversed. For both purposes, the **E**-field must be strong enough, typically 2 kV/cm, its reversal must be accurate and its direction precisely aligned along the beam and cell axis.

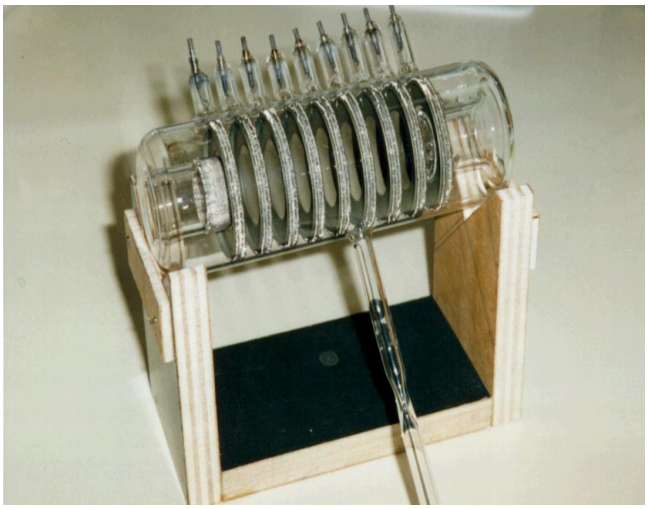

Fig. 3. A glass cell with internal electrodes for application of a longitudinal electric field. At each end, an electric bracelet, slipped around the re-entrant window and connected to the extreme electrode, forces the inner surface of the window to the potential of the electrode.

The use of a cell gives access to very high atomic densities and hence high number of excited atoms, otherwise unachievable in beam or trap experiments. As an important consequence, the electric field has to be pulsed so as not to initiate a discharge in the vapor (pulse duration $\ll 1$ μs). Nevertheless, the **E**-field acts as a static field for the atoms, provided that it lasts much longer than the 20 ns pump and probe laser pulses. A typical pulse duration is 150 ns.

The first steps of the PV experiment have been carried out with glass cells [7]. The motivations for a radical change are the limitations encountered with those cells in our demanding experimental conditions: an intense laser pulse at 540 nm (15 ns, 2 mJ/mm^2), a longitudinal electric field (2 kV/cm over 10 cm, *i.e.* 20 kV), a rather high cesium density ($N_{Cs} \sim 2 \times 10^{14}$ at/cm^3), and a high cell temperature (ideally above 200 °C). Let us summarize the four main limitations of glass cells.

(i) It has been shown [8] that the internal surface of glass cells becomes conductive in presence of the cesium vapor. The first consequence is that *internal* electrodes must be implemented to produce an **E**-field in glass cells (see Fig. 3). This is a technological complication, especially if one needs a highly uniform electric field [8], and dramatically impedes changes of the **E**-field configuration. Furthermore, resistive currents develop on the inner walls of the cell when the high voltage (HV) is applied, and these lead to unwanted magnetic fields and potential

systematic effects. In particular a magnetic field with a component along the longitudinal axis is dangerous when it is odd under the **E**-field reversal.

(ii) The equilibrium population of cesium dimers Cs_2 leads to a plasma $Cs^+ + e^-$ *via* a two-step photo-ionization process involving two 539 nm photons [9]. In the longitudinal **E**-field, the electrons are quickly accelerated towards the windows, and the nearly static Cs^+ ions give rise to a stray transverse electric field, yielding an unwanted 6S−7S Stark induced transition amplitude [10]. These dimers are thermally dissociated if the vapor is overheated but, above 200 °C, the glass cells develop a brownish coloration characteristic of the irreversible reduction of SiO_2 by the alkali vapor, producing a thin layer of silicon.

(iii) With both the pump laser pulse and the longitudinal Stark **E**-field, the optical transmission of a glass cell falls dramatically after a few tens of hours. This is hardly compatible with the long averaging times required for a precise Parity Violation measurement. The effect, localized to the region of laser impact, comes from the bombardment of the glass windows by the above mentioned electrons and Cs^+ ions. Moreover the photoelectric effect of the Cs atoms adsorbed at the window surface tends to reinforce the process.

(iv) The reflection of the excitation laser pulse by the exit window of the cell is a potential source of systematic effect in the PV measurement. One solution is to use windows made of highly parallel plates to control and cancel the reflection by temperature tuning of the interference order (Sect. 5.2). In glass cells this possibility is quickly lost, due to the damage to the windows mentioned in (iii).

The optical, electrical, and thermal properties of sapphire make it a good candidate to overcome these limitations.

3 Electrical conductivity of cesium cells and relaxation of a DC field

The surface electrical conductivity of glass and sapphire cells has been investigated and is reported in [11]. Let us briefly recall the main conclusions. There is a drastic difference of behavior as exhibited by glass and monocrystalline sapphire cells exposed to a dry vapor of cesium. Before use in the PV experiment, the best sapphire cell had a square resistance of order of 1 GΩ, to be compared with a few tens of kilo-ohms for glass cells. Let us mention that when the square resistance of the inner walls of sapphire cells is measured after use on the PV experiment, one finds the value has dropped down to a few megohms, whatever the initial value, but still remains 2 to 3 orders of magnitude larger than that of glass cells.

The electric field produced inside the cell with external electrodes decays with a time constant $\tau = RC$, where R and C are the effective resistance and capacitance in the simplest model. We want τ to be much larger than the laser pulse duration ($\simeq$ 20 ns), *i.e.* $\tau \geq 100$ ns, so that with the typical value $C = 1$ pF, the requirement is $R \geq 100$ kΩ. We conclude that to produce such a field with glass cells, one must use internal electrodes. With sapphire cells, on the other hand, this becomes possible using external electrodes.

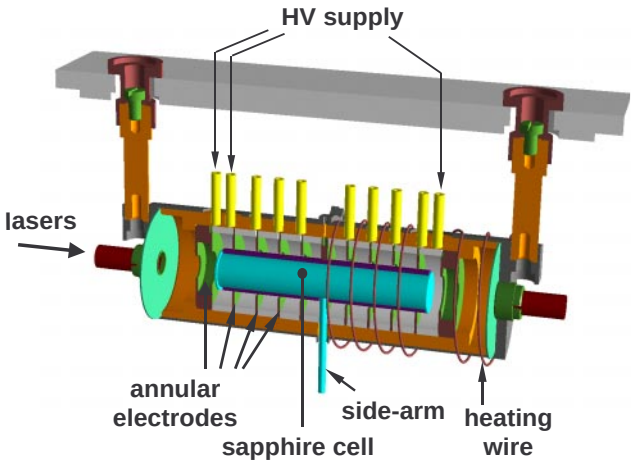

Fig. 4. The oven assembly containing the sapphire cell and the HV electrodes.

4 Implementation

4.1 Mechanics

Figure 4 represents the oven we designed in order to hold the cell, heat the body and produce the longitudinal electric field inside.

The body of the cell[1] consists of a monocrystalline cylindrical sapphire tube ($L = 82.7$ mm, $\phi_{\rm int} = 10$ mm, $\phi_{\rm ext} = 13$ mm) with two windows ($\phi = 15$ mm, $e = 0.5$ mm) glued at the ends. The c-axes of both windows and the tube are aligned along the tube axis. A sapphire side-arm (length 40 mm) is glued in the middle of the main tube, and is terminated by a sealed molybdenum glass tube (length 30 mm). The bottom of the glass tube contains a few mm^3 of liquid cesium.

The body of the sapphire cell is nested in two pieces of silica forming a tube, which is placed into a set of eleven annular electrodes (gold-plated ARCAP) and ten silica spacers. The over-heating of the vapor necessary first to have a dry vapor, and second to thermally destroy the Cs_2 dimers, is achieved with a non-magnetic cylindrical oven made of titanium ($\phi_{\rm int} = 44$ mm, length 144 mm, $e = 1$ mm), around which is glued[2] a bifilar heating wire (see Fig. 4). Attention has been paid to avoid metal-metal contacts and associated thermocouples, since they are sources of uncontrolled thermoelectric currents and hence magnetic fields.

Thanks to the long side-arm, the cesium droplet can be kept at a temperature in the range 140−150 °C to

[1] The cell is constructed [12] by Sarkisyan's group at the Institute of Physics in Ashtarak (Armenia).

[2] Ceramabond 571: refractory, non-conductive glue, AREMCO Products, Inc.

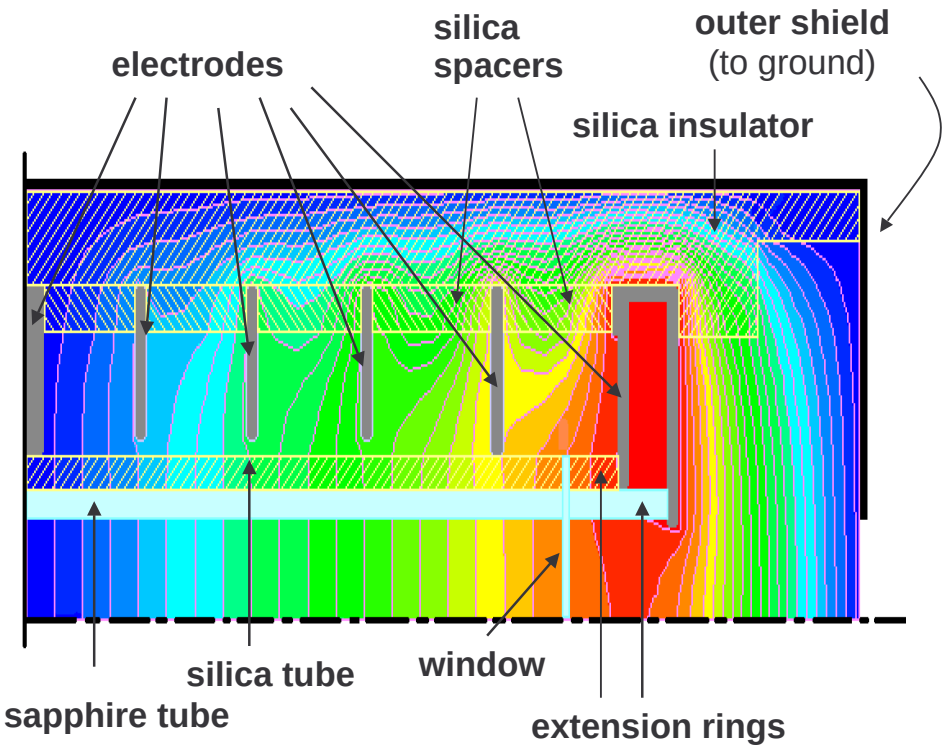

Fig. 5. Calculated equipotentials for a quarter of the oven assembly, showing the distribution along the longitudinal ($z = 0$ to 72 mm) and radial ($r = 0$ to 21 mm) directions.

produce the vapor density in the range 1 to 2 $\times 10^{14}$ cm^{-3}, while the body of the cell is overheated up to 350 °C. The oven has small orifices ($\phi = 8$ mm) for beam passage, so that using thermal screens we could avoid the insertion of optical windows.

Because of the requirements of the PV experiment [7], the mechanical design has to preserve as much as possible the cylindrical symmetry around the cell axis. The only two exceptions are due to the necessary side-arm and the electric wires feeding the electrodes with the required high voltage. The vertical plane of symmetry is preserved.

4.2 Electrostatic calculations

Choosing electrode and cell configuration of cylindrical symmetry favors the realization of a highly homogeneous field. The reason comes from the symmetry properties of the Laplace's equation written in cylindrical coordinates which implies $\partial V/\partial r = 0$ for $r = 0$. The radial electric field in the interaction region chosen along the symmetry axis should *a priori* be very small. If, in addition, the electrodes and potentials respect the invariance by translation, then one can expect excellent homogeneity of the longitudinal field component along the axis. In practice translational invariance is only approximately realized and optimization of a suitable geometry relies on a numerical calculation of the equipotentials when the electrodes are supplied with arithmetically growing potentials $(-HV, -4HV/5, ..., +4HV/5, +HV)$. Our two dimensional numerical simulation starting from a discretization of the Laplace's equation in cylindrical coordinates uses the "simultaneous over relaxation method" described in [13]. It takes into account the presence of the dielectric constants of both the anisotropic sapphire (body and windows) and the insulators around it[3], by discretizing the continuity relations at the boundaries between different dielectrics. The equipotentials calculated with a grid of 600 × 600 points are drawn in Figure 5 for a quarter of the cell and oven. Notice in particular that the edge effects at the tube ends are efficiently attenuated thanks to (i) the position and shape of the extreme electrode, and (ii) the placement at both ends of the cell of sapphire and silica extension rings.

The local variations of E_z along the cell axis do not exceed 10^{-2}. In the whole interaction region (typical laser beam diameters are $\phi_{\rm pump} = 2$ mm, and $\phi_{\rm probe} = 1.4$ mm), the RMS fractional variation of E_z is 3×10^{-4} and the RMS radial field $8 \times 10^{-4} \langle E_z \rangle$.

4.3 Production of the reversible high voltage pulses

The last step is the production of reversible HV pulses for the 11 electrodes. As Figure 6a schematizes, this is achieved with

- a capacitor charging power supply (FUG, Model HCK200-12500) delivering stabilized DC voltages up to 12.5 kV;

[3] $\epsilon_{\|} = 10.6$, $\epsilon_{\perp} = 8.6$ for sapphire, and $\epsilon = 3.7$ for silica, all constant up to 200 °C in the range 1–10 MHz.

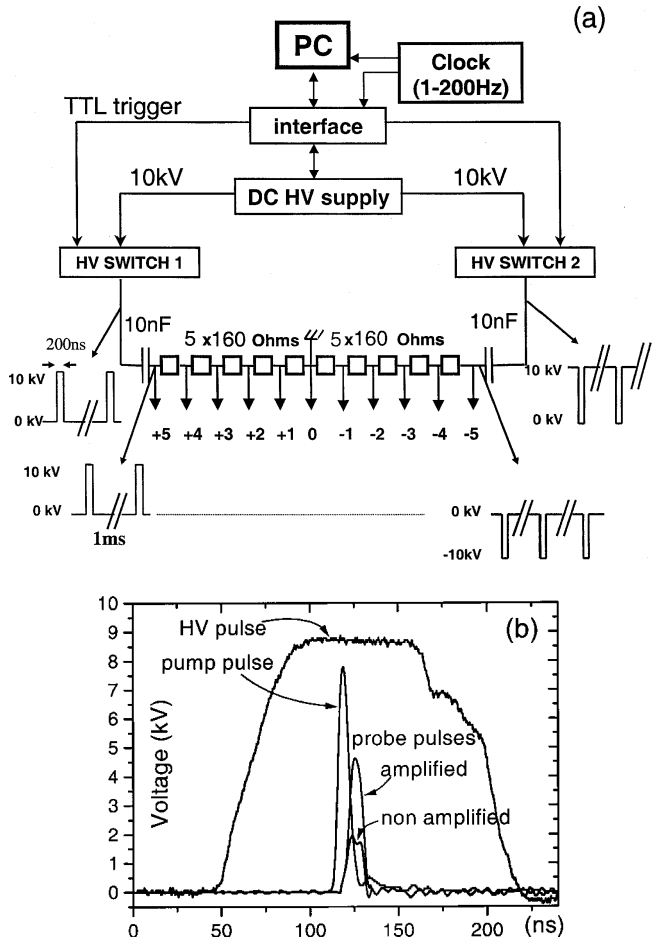

Fig. 6. (a) Scheme for production of the reversible HV pulses. (b) Temporal shape of the HV pulse. The laser pulses give the timescale of the experiment.

- two solid-state HV switches (DEI, Model GRX-10K-H) with duration adjustable from 200 ns to DC and rising and falling times < 60 ns);
- two decoupling capacitors ($C_{\text{decoupling}} = 10$ nF);
- a ten resistor bridge ($10 \times (R = 160\ \Omega)$, non inductive carbon resistors).

The two switches are gated so as to provide 10 kV pulses of same polarity, but with complementary duty-cycle (gate signal #1 is high when #2 is low, and *vice versa*). The decoupling capacitors filter the DC component, so that at their output we obtain short 10 kV pulses of opposite signs with temporal shape shown in Figure 6b. The short pulses are positive on side #1, when they are negative on side #2, allowing for a potential decreasing arithmetically from $+HV$ on electrode $\#+5$ to $-HV$ on electrode $\#-5$. Then, by simply exchanging the duty cycles of the two switches, one can reverse the signs of the HV pulses applied to the electrodes.

This duty cycle exchange has to occur only when the switches are not charged, otherwise a long (> 600 ns) HV pulse is transmitted to the electrodes and would lead to a discharge in the vapor. So we need to discharge the DC input of each switch. The discharge must be sufficiently slow (~ 3 ms) so as to be efficiently filtered by the decoupling capacitors. The 50 nF entrance capacitors of the switches have then to be recharged to 10 kV, and the charge duration is governed by the current available from the DC supply (30 mA). The minimum reversal time reaches then about 50 ms.

A long reversal time is a limitation if one wants to reverse the **E**-field at each clock pulse (repetition rate 120 Hz), but in our experiment, it is sufficient for us to reverse **E** at 4 Hz.

This set-up produces the required pulses and HV-reversals provided two conditions are fulfilled:

(i) $5RC_{\text{decoupling}} \gg \tau_{\text{pulse}}$,
i.e. the charge of the decoupling capacitors has to remain constant during the short pulse duration;

(ii) $4RC_{\text{parasitic}} \ll \tau_{\text{pulse}}$,
i.e. the parasitic capacitance between the electrodes and the oven ($C_{\text{parasitic}} \simeq 2$ pF) must be charged quickly compared to the pulse duration. Both conditions are fulfilled with the values given above.

Because of (ii), low resistance values are needed, which leads to high peak dissipated power (25 kW for $R = 160\ \Omega$, and $HV = 10$ kV), but the small duty cycle (2×10^{-5}) allows to a reasonable mean power of order 0.5 W.

5 Experimental results

In this section we review the main changes in operating conditions which have resulted from our using sapphire cells with external electrodes in place of glass cells with internal electrodes.

5.1 Magnitude of the electric field inside the sapphire cell

Our primary concern was to verify the magnitude of the field generated by the external electrodes. To that purpose atomic signals prove a convenient probe. The longitudinal **E**-field produces a Stark transition dipole, $\mathbf{d}^{\text{Stark}}_{6S-7S}$, between the 6S and 7S states, and the transition rate τ grows as $|\mathbf{d}^{\text{Stark}} \cdot \hat{\boldsymbol{\epsilon}}_{\text{L}}|^2 \propto \beta^2 \mathbf{E}^2$, where $\hat{\boldsymbol{\epsilon}}_{\text{L}}$ is the pump laser field, and β is the transition tensor polarizability[4]. The population in the 7S level also grows like $\mathbf{E}^2$, and in the simplest model, the intensity of the probe beam pulse, amplified by stimulated emission, grows exponentially while propagating in the excited vapor, $I(L) = I(0)\mathrm{e}^{kL}$ with $k \propto \mathbf{E}^2$ (see [14] for details). In practice, the amplification (of the order of unity) is slightly decreased by a small non resonant background (a few percent) of collisional origin.

[4] The small PV dipole originating from weak interactions is completely negligible in this discussion, as well as the forbidden M_1 dipole. In these conditions, we have $\mathbf{d}^{\text{Stark}}_{6S-7S} = -\alpha\mathbf{E} - \mathrm{i}\beta\boldsymbol{\sigma} \times \mathbf{E}$, where α and β are the scalar and tensorial polarizabilities. The scalar part plays no role for a $6S_F \rightarrow 7S_{F'}$ transition when $F \neq F'$. When **E** is along the beam, the scalar dipole plays no role whatever the chosen hyperfine component.

Table 1. Typical parameters in sapphire cells for the two pump-probe transitions used ("3–4–5" means $6S_{F=3} \rightarrow 7S_{F=4} \rightarrow 6P_{3/2F=5}$, and "3–4–4" means $6S_{F=3} \rightarrow 7S_{F=4} \rightarrow 6P_{3/2F=4}$).

transition	excitation energy (mJ/pulse)	probe power (mW)	pump waist (mm)	probe waist (mm)	N_{Cs} (at/cm^3)
3−4−5	1.0 ± 0.05	0.34 ± 0.02	1.0 ± 0.03	0.70 ± 0.02	$1.0 \pm 0.07 \times 10^{14}$
3−4−4	1.8 ± 0.05	0.48 ± 0.02	1.0 ± 0.03	0.70 ± 0.02	$1.0 \pm 0.07 \times 10^{14}$

Table 2. Optical densities $\mathcal{A} \equiv \ln(I^{amp}/I^{ref})$ (corrected for the background mentioned in text) obtained in a glass and in a sapphire cell for each of the four experimental configurations. The $\mathcal{A}$ values are normalized to common values of the experimental parameters involved: pump beam energy 1 mJ/pulse, $N_{Cs} = 10^{14}$ at/cm^3, extrapolation to zero saturation and same beam waists as in Table 1.

transition	polarizations	$\mathcal{A}^{Glass}$	$\mathcal{A}^{Sapph}$	$\sqrt{\mathcal{A}^{Sapph}/\mathcal{A}^{Glass}}$
3−4−5	$\hat{\epsilon}^{pr} \perp \hat{\epsilon}^{exc}$	1.18 ± 0.18	1.42 ± 0.21	1.1 ± 0.13
3−4−5	$\hat{\epsilon}^{pr} \parallel \hat{\epsilon}^{exc}$	0.90 ± 0.14	1.13 ± 0.17	1.12 ± 0.13
3−4−4	$\hat{\epsilon}^{pr} \perp \hat{\epsilon}^{exc}$	0.22 ± 0.03	0.22 ± 0.03	1.00 ± 0.12
3−4−4	$\hat{\epsilon}^{pr} \parallel \hat{\epsilon}^{exc}$	0.81 ± 0.12	0.77 ± 0.12	0.98 ± 0.12

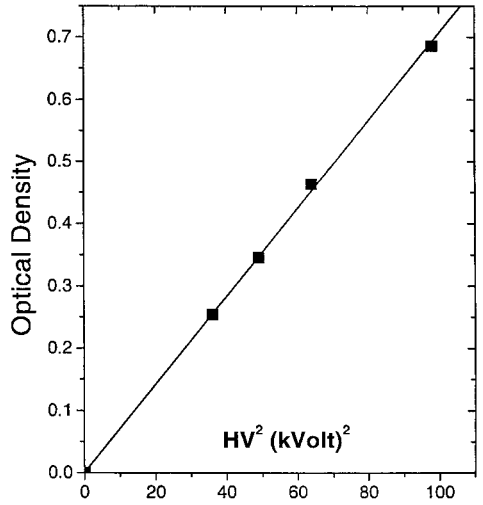

Fig. 7. Measured probe optical density *versus* the voltage applied to the electrodes squared (transition 3–4–4, beam polarizations $\hat{\epsilon}^{pr} \perp \hat{\epsilon}^{exc}$). Values of $\mathcal{A}$ are corrected for the small background (see text). The solid line is a linear fit.

Experimentally, we measure the optical density $\mathcal{A} = kL$ for the probe beam from $\mathcal{A} \equiv \ln(I_{pr}^{amp}/I_{pr}^{ref})$, where I_{pr}^{amp} [I_{pr}^{ref}] is the intensity of the probe beam after propagation in the vapor with [without] a pump pulse tuned to resonance for the 6S−7S transition (see the time sequence in Fig. 2). This same quantity is then measured with the pump pulse detuned so that the background can be determined and subtracted.

Figure 7 shows that $\mathcal{A}$ (after the background subtraction) scales like E^2, as expected. This relation of proportionality can be exploited to deduce the value of the electric field from the measurements of the optical density provided the existence of a calibration. In our glass cells, the Stark field was produced with internal electrodes, so that its magnitude can be computed knowing the geometry and potentials applied to the electrodes. Therefore we can determine the electric field applied to the atoms in the sapphire cells by comparing the optical density for the probe beam in the two kinds of cell. The proportionality factor $\mathcal{A}/E^2$ involving several experimental parameters, it is crucial to perform the comparison in very similar experimental conditions. Explicitly, we have:

$$\mathcal{A} \propto \Phi^{exc} N_{Cs} \eta_{sat} f_{coll} E^2 L$$

where Φ^{exc} is the energy density per pulse of the pump laser, N_{Cs} the 6S atom density, η_{sat} a factor which accounts for the saturation of the probe amplification (which depends on the transition and on the polarizations), L the length of the cell. The factor f_{coll} accounts for slight departure from linear dependence of $\mathcal{A}$ with N_{Cs} because of collisional line broadening.

The comparison has been done for the pump beam tuned to the $6S_{F=3} \rightarrow 7S_{F=4}$ resonance frequency and two probe hyperfine components, $7S_{F=4} \rightarrow 6P_{3/2F=5}$ and $7S_{F=4} \rightarrow 6P_{3/2F=4}$, which have very different gains and saturation behaviors. We measure the optical density $\mathcal{A}$ with pump and probe polarizations either parallel or orthogonal[5].

The typical conditions for the two transitions are given in Table 1 and the optical densities, after normalization to common values of the parameters, in Table 2. We calculate the factor $\sqrt{\mathcal{A}^{sapph}/\mathcal{A}^{glass}}$ for the four experimental configurations, and since those values are in reasonable agreement within the uncertainties, we take the average and we deduce the value of the electric field in the sapphire cell from:

$$E(\text{sapph}) = E(\text{glass}) \left\langle \sqrt{\frac{\mathcal{A}^{sapph}}{\mathcal{A}^{glass}} \times \frac{L^{glass}}{L^{sapph}}} \right\rangle .$$

The length of cesium column for the two cells are respectively $L^{glass} = 86.9$ mm, and $L^{sapph} = 82.7$ mm. We thus

[5] The linear pump polarization creates an anisotropy (an alignment) in the excited state, resulting in a linear dichroism for the probe pulse, hence different gains for $\hat{\epsilon}^{exc} \parallel \hat{\epsilon}^{pr}$ and $\hat{\epsilon}^{exc} \perp \hat{\epsilon}^{pr}$.

finally obtain $E(\text{sapph}) = 2.05 \pm 0.25$ kV/cm, in agreement with the electrostatic calculated value of 1.85 kV/cm for the voltages applied. The 12% precision is limited by the uncertainty in the determination of the parameters involved in $\mathcal{A}$. In particular the reflection coefficients of both windows at the pump and probe wavelengths, and for each type of cell, are needed in order to determine the actual intensities inside the two cells.

The agreement between the results from the four experimental configurations constitutes a valuable cross-check since they have different sensitivity to the numerous experimental parameters that have to be taken into account.

By translating the oven-and-cell assembly in transverse direction with respect to the beams, we checked that the longitudinal **E**-field inside the sapphire cell is homogeneous at the 1% level over a $\phi = 5$ mm region around the cell axis.

We notice that the values of the optical density, and hence of the electric field, are the same when we measure them in a fresh cell, and after several hundreds of hours of effective operation. This is an important check, since the conductivity of the sapphire cell is different before and after use (see Sect. 3).

5.2 Optical properties of the windows

The windows of our new cells are also made of monocrystalline sapphire. First, unlike glass windows, the present sapphire windows remain intact in presence of the aggressive cesium vapor, after several hundreds of hours of exploitation in the PV experimental conditions (see (iii) in Sect. 2). Second, we have been able to implement an efficient control of the reflection of those windows, simply by tuning the window temperature. Indeed, each window constitutes a plane parallel Fabry-Perot etalon, provided one selects thin plates (500 μm) with excellent parallelism, and very low surface roughness. The interesting point for the PV experiment is the inhibition of the reflection of the pump laser on the *exit* window of the cell. We can lower this reflection below 1% with a control of the cell temperature at the 0.5 °C level. See [16] for details.

5.3 Thermal dissociation of the dimers

The sapphire cells can be heated up to very high temperatures [17]. Our set-up is designed to heat the body of the cell, and hence the vapor, up to 400 °C, and we have made measurements up to 340 °C. The typical temperatures are $T_{\text{reservoir}} = 141$ °C, and $T_{\text{body}} = 250$ °C. In these conditions, we have $N_{Cs_2} = 0.7 \times 10^{10}$ cm^{-3}, instead of $N_{Cs_2} = 4.8 \times 10^{10}$ cm^{-3} with the same reservoir temperature and $T_{\text{body}} = 175$ °C in glass cells. An atomic signal that confirms the reduction of the dimer density is the absorption of the probe laser, resonant for $6P_{3/2}-7S$, *vs.* pump-probe delay, with pump laser detuned from the $6S-7S$ transition and **E**-field not applied [9]. The Cs_2 dimers lead to excited $6P_{3/2}$ Cs atoms, *via* dimer photodissociation

$$Cs_2 + \gamma(540\text{ nm}) \rightarrow Cs(5D_{5/2}) + Cs(6S),$$

followed by the decay of $Cs(5D_{5/2})$ atoms towards the $6P_{3/2}$ level

$$Cs(5D_{5/2}) \rightarrow Cs(6P_{3/2}) + \gamma(3.49\ \mu\text{m}).$$

The second step is long ($\tau_{5D} \sim 1.2$ μs), and the maximum absorption is for a pump-probe delay around 2 μs[6]. In Figure 8a the absorption of the probe pulse is plotted *vs.* pump-probe delay for two vapor temperatures: $T_{\text{body}} = 177$ °C, and $T_{\text{body}} = 242$ °C, the reservoir temperature being kept constant at 151 °C. Figure 8b shows

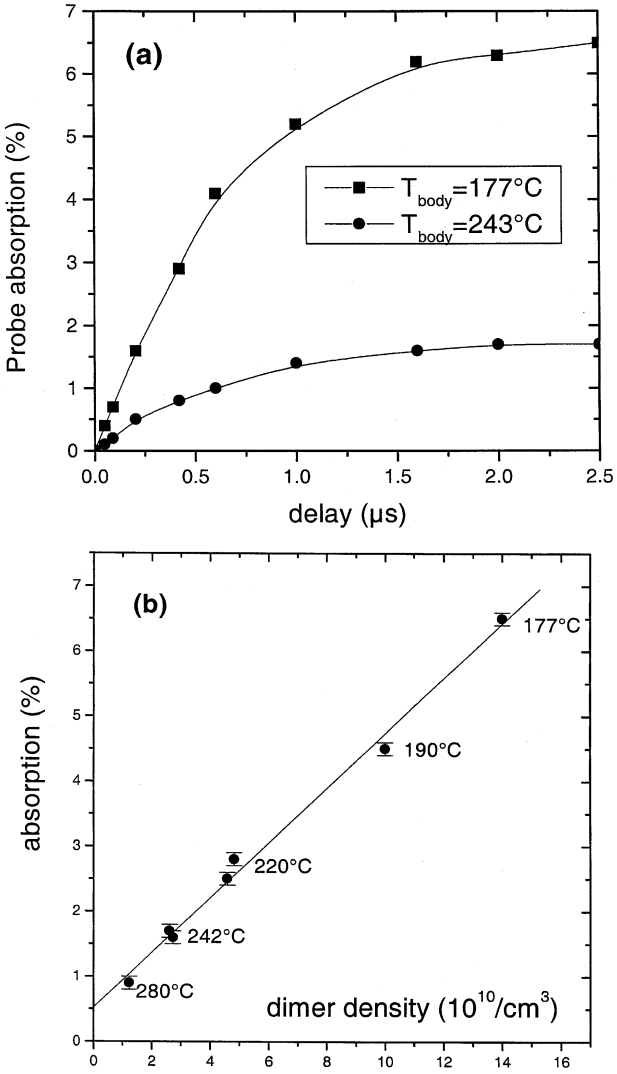

Fig. 8. (a) Absorption of the probe pulse *vs.* pump-probe delay for two vapor temperatures, 242 °C and 177 °C, pump detuned from the 6S–7S transition. Solid curves are guidelines. (b) Maximum absorption *versus* dimer density, when T_{body} is changed from 177 °C to 280 °C at constant side-arm temperature $\simeq$151 °C. The solid line is a linear fit with a small non zero value at $N_{Cs_2} = 0$, attributable to a 6S–5D Raman transition.

[6] The lifetime of the 6P population is 5 μs due to resonance radiation trapping.

the maximum absorption *versus* the dimer density. When $T_{\rm body}$ is varied in the range [177 °C, 280 °C], we observe an almost linear dependence, which confirms the expected dimer thermal destruction. The small non-zero value at $N_{\rm Cs_2} = 0$ is attributable to the $6S_{1/2}-5D_{5/2}$ Raman transition producing $5D_{5/2}$ atoms from ground state atoms, by absorption of a pump photon at 540 nm, followed by emission of an infrared photon [18].

5.4 Photoinduced E-field assisted electron emission

A detrimental property of sapphire surfaces is encountered which cannot be ignored at least for our PV experiment. This is connected with a so called exo-electron emission of the surface of sapphire, here photoinduced and field-assisted [19].

Given the homogeneity of the field created by the electrodes, existence of transverse fields is unambiguously imputable to the presence of free charges inside the cesium vapor. By exploiting the properties of the 6S−7S Stark induced dipole, we can measure and map the presence of transverse **E**-field and **B**-field components. We do observe a radial centripetal **E**-field and an orthoradial **B**-field, respectively even and odd under reversal of the HV applied to the electrodes. The saturation of these fields occurs for low pump intensity (0.2 mJ/mm^2). These $(\mathbf{E}_\perp, \mathbf{B}_\perp)$ fields are consistent with an electronic space charge accelerated in the longitudinal **E**-field (typical values 20−30 V/cm and 5−10 mG per mm off axis). Furthermore, by applying directly the HV to the windows rendered conductive using an ITO (tin doped indium oxide) transparent surface deposition on their outer side, we do detect a pulse of current flowing through the windows[7] just as the pump laser pulse is established. This proves that the electron emission is a photoinduced process initiated at the window surface. Comparison of the current pulse at anode and cathode windows indicates large multiplication (≥ 10) of the charges in between the windows, most probably by secondary emission from electron collisions at grazing incidence on the sapphire tube [20].

6 Further extension

The previous results have an important consequence: they open the possibility of realizing pump-probe beam experiments in a *transverse* **E**-field. With internal electrodes, the detection method based on probe beam amplification by stimulated emission cannot be exploited since the collinear pump and probe beams necessarily pass through regions where the **E**-field is very inhomogeneous. With a sapphire cell and external electrodes, this difficulty vanishes completely: a homogeneous transverse field can be applied along the whole length of vapor column provided that the electrodes are longer than the cell. For a long cell (length $\gg$ diameter), the transverse geometry has further advantages. For a given field magnitude, the required potential is much weaker since the distance between the two transverse electrodes can be much smaller. Additionally, the required potential becomes independent of the cell length. The latter can thus be increased at will with a view to enhance the vapor amplification and hence the efficiency of the pump-probe detection method [14]. Up to now, PV experiments in transverse field have been performed using fluorescence detection only [5]. It is of interest to test whether better signal-to-noise ratio can be achieved by using detection *via* probe amplification.

On the other hand, the photoinduced exoelectron emission and its multiplication should be less efficient in the transverse field configuration. Whatsoever fuller information about these processes should be obtained.

[7] The electron flow is stopped on the inner side, but due to efficient capacitive coupling, an image charge develops on the (conductive) outer side.

7 Conclusion

We described the implementation of a cesium sapphire cell on our PV experimental set-up. We take advantage of the low electric conductivity of the sapphire tube in presence of the cesium vapor to control an electric field inside the cell with external electrodes. The presence of the electric field of expected value in the cell was directly checked *in situ* on atomic signals by exploiting the 6S–7S Stark-induced transition. The new oven assembly also allows for thermal destruction of the Cs_2 dimers, and thanks to windows of high optical quality, a good control of the reflectivity is obtained by tuning the window temperature. An interesting extension of this work consists in the detection of the 6S–7S transition by probe beam amplification in the transverse field configuration. We are presently engaged in the implementation of this situation.

We thank Dr. A.V. Papoyan for experimental contributions to this work. We are grateful to the Ministère de l'Enseignement Supérieur et de la Recherche for providing E. Jahier with a student grant.

References

1. M.A. Bouchiat, J. Guéna, Ph. Jacquier, M. Lintz, M.D. Plimmer, Z. Phys. D **33**, 89 (1995).
2. S.I. Kanorsky, A. Weis, J. Skalla, Appl. Phys. B **60**, S165 (1995).
3. S. Chu, Rev. Mod. Phys. **70**, 685 (1998); W.D. Phillips, Rev. Mod. Phys. **70**, 721 (1998).
4. Special issue, Eur. Phys. J. D **7** (1999).
5. M.A. Bouchiat, C. Bouchiat, Rep. Prog. Phys. **60**, 1351 (1997).
6. L.R. Hunter, Science **252**, 73 (1991).
7. J. Guéna, D. Chauvat, Ph. Jacquier, M. Lintz, M.D. Plimmer, M.A. Bouchiat, Quant. Semiclass. Opt. **10**, 733 (1998).
8. L. Pottier, M.A. Bouchiat, J. Guéna, M. Lintz, E. Hughes, Ph. Jacquier, Meas. Sci. Technol. **2**, 1147 (1991).
9. M.A. Bouchiat, J. Guéna, Ph. Jacquier, M. Lintz, Chem. Phys. Lett. **199**, 85 (1992).

10. M.A. Bouchiat, J. Guéna, Ph. Jacquier, M. Lintz, Opt. Commun. **104**, 157 (1993).
11. M.A. Bouchiat, J. Guéna, Ph. Jacquier, M. Lintz, A.V. Papoyan, Appl. Phys. B **68**, 1109 (1999).
12. D.G. Sarkisyan, A.V. Melkonyan, Prib. i Tekhn. Ekspe. **2**, 202 (1989).
13. W.H. Press, S.A. Teukolsky, W.T. Vetterling, B.P. Flannery, *Numerical Recipes* (Cambridge Univ. Press, 1986).
14. C. Bouchiat, M.A. Bouchiat, Z. Phys. D **36**, 105 (1996).
15. J. Guéna, D. Chauvat, Ph. Jacquier, M. Lintz, M.D. Plimmer, M.A. Bouchiat, J. Opt. Soc. Am. B **14**, 271 (1997).
16. E. Jahier, J. Guéna, Ph. Jacquier, M. Lintz, A.V. Papoyan, M.A. Bouchiat, Appl. Phys. B **71**, 1 (2000).
17. D.H. Sarkisyan, A.S. Sarkisyan, A.K. Yalanusyan, Appl. Phys. B **66**, 241 (1998).
18. R. Wyatt, D. Cotter, Appl. Phys. **21**, 199 (1980).
19. L. Oster, V. Yaskolo, J. Haddad, Phys. Stat. Sol. (a) **174**, 431 (1999); P. Iacconi, D. Lapraz, R. Bindi, M. Benabdesselam, Phys. Stat. Sol. (a) **163**, 337 (1997).
20. J. Cazaux, Ultramicroscopy **60**, 411 (1995); J. Cazaux, in *Ionization of Solids by Heavy Particles*, edited by R.A. Baragiola, NATO ASI Ser. B **306**, 325 (1993); J. Cazaux, P. Lehuede, J. Electron. Spectrosc. Relat. Phenom. **59**, 49 (1992).